PAPER Special Section on Nonlinear Theory and Its Applications

A Study of the Pendulum Equation with a Periodic Impulsive Force — Bifurcation and Control —

Tetsushi UETA†, Hiroshi KAWAKAMI†, *Members, and* Ikuro MORITA†, *Nonmember*

SUMMARY The pendulum equation with a periodic impulsive force is investigated. This model described by a second order differential equation is also derived from dynamics of the stepping motor. In this paper, firstly, we analyze bifurcation phenomena of periodic solutions observed in a generalized pendulum equation with a periodic impulsive force. There exist two topologically different kinds of solution which can be chaotic by changing system parameters. We try to stabilize an unstable periodic orbit embedded in the chaotic attractor by small perturbations for the parameters. Secondly, we investigate the intermittent drive characteristics of two-phase hybrid stepping motor. We suggest that the unstable operations called pull-out are caused by bifurcations. Finally, we proposed a control method to avoid the pull-out by changing the repetitive frequency and stepping rate.

key words: *impulsive force, bifurcation, controlling chaos, stepping motor*

1. Introduction

The equation of motion for a kicked rotor, a stepping motor, a circuit containing a Josephson junction with an impulsive voltage source is described as a second order differential equation containing a sinusoidal function with a discontinuous external force. In such systems, two topologically different kinds of periodic solutions are found; revolving and oscillatory solution. The former winds around a cylindrical phase space, and latter does not, see Fig. 1. We observed higher periodic orbits or chaotic states for both these solutions.

In this paper, we investigate some properties of the pendulum equation with a periodic impulsive force. First of all, we analyze periodic orbits by using bifurcation theory. Although this equation has an impulsive force, i.e., the orbit changes discontinuously, we can calculate bifurcation parameters since its Poincaré mapping is constructed as a differentiable map [1]. As the result, some properties of the periodic solutions are explained from bifurcation diagrams. In Sect. 5 we propose a method to stabilize the unstable periodic orbit embedded in a chaotic attractor by small perturbations of the system parameter.

The equation is also described the behavior of a stepping motor on the velocity error plane. Especially if the orbit converges to any revolving orbit the motor cannot be controlled to generate the desirable velocity. In Sect. 6.2, we study the bifurcation phenomena of periodic orbit in case that the motor is driven by intermittent sequences [2], and obtain the bifurcation diagram. Moreover in Sect. 6.3 we propose a method to avoid the pull-out and to improve the transient responses by changing the repetitive frequency and stepping rate of the intermittent drive sequence.

Manuscript received January 31, 1995.

†The authors are with the Faculty of Engineering, The University of Tokushima, Tokushima-shi, 770 Japan.

2. Mathematical Model

The motion of a pendulum with damping is described by the following autonomous equation:

$$\begin{aligned} \frac{dx}{dt} &= y &&= f(x,y) \\ \frac{dy}{dt} &= -\kappa y - \sin x &&= g(x,y) \end{aligned} \tag{1}$$

where, $(x,y) \in \boldsymbol{R}^2$ is the state, $\kappa > 0$ is a damping coefficient. Note that the state space is regarded as $S^1 \times \boldsymbol{R}$, where $S^1 = \{x \in \boldsymbol{R} \bmod 2\pi\}$. Since the system (1) is dissipative, there is no periodic solution except for $k = 0$. Now we assume an input which achieves the periodic discontinuity of initial state by using the sequence of impulses. Then Eq. (1) is rewritten as follows:

$$\frac{dx}{dt} = f(x,y) + \frac{\pi}{2} h \sum_{k=0}^{\infty} \delta(t - k\tau)$$

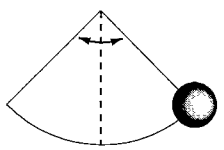

Oscillatory solution

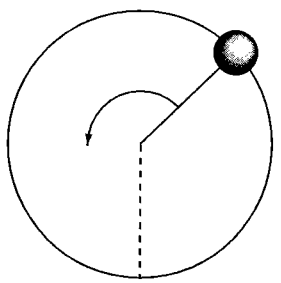

Revolving solution

Fig. 1 Oscillatory solution and revolving solution.

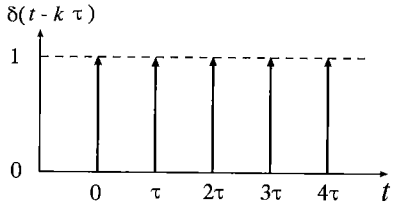

Fig. 2 Sequence of implusive waves $\sum_{k=0}^{\infty} \delta(t - k\tau)$.

$$\frac{dy}{dt} = g(x, y) \tag{2}$$

where, $\delta(t)$ is the Dirac's delta function, and h, τ are height and interval of the impulse, respectively. See Fig. 2. $\pi/2$ is added for the convenience sake.

Adding the periodic impulsive force to $f(x, y)$ is frequently assumed to simulate the response of the periodically stimulated neuron model by a BVP oscillator [3].

3. Poincaré Mapping

We construct the Poincaré mapping to analyze periodic solutions observed in Eq. (2) in $h > 0$. The impulsive external force affects the orbit of Eq. (2) as an instantaneous translation. The computational method to obtain periodic points and bifurcation parameters for the periodic solution driven by a discontinuous input are already proposed [1], hence the bifurcational analysis for oscillations observed in this system is possible. In the following, we summarize this scheme briefly.

We rewrite the Eq. (2) as the following form:

$$\frac{d\boldsymbol{x}}{dt} = \boldsymbol{f}(t, \boldsymbol{x}, \lambda) + \boldsymbol{h} \sum_{k=0}^{\infty} \delta(t, \tau) \tag{3}$$

where, $\boldsymbol{x} \in \boldsymbol{R}^n$ and $\lambda \in \boldsymbol{R}$ are the state and the system parameter, respectively. Suppose $\boldsymbol{f} : \boldsymbol{R} \times \boldsymbol{R}^n \times \boldsymbol{R} \to \boldsymbol{R}^n$ is C^∞. Let a solution of Eq. (2) be

$$\boldsymbol{x}(t) = \varphi(t, \boldsymbol{x}_0, \lambda) \tag{4}$$

where,

$$\boldsymbol{x}(0) = \varphi(0, \boldsymbol{x}_0, \lambda) = \boldsymbol{x}_0. \tag{5}$$

We choose the interval of the Poincaré mapping as a period τ of the impulse sequence. In the moment at which the impulse is added to the system, a composition of the following two maps is considered as the Poincaré mapping; P_1 is a map which translates $\boldsymbol{x}$ to $\boldsymbol{x} + \boldsymbol{h}$:

$$\begin{aligned} P_1 : \boldsymbol{R}^n &\to \boldsymbol{R}^n \\ \boldsymbol{x} &\mapsto \boldsymbol{x} + \boldsymbol{h} = \boldsymbol{x}_1. \end{aligned} \tag{6}$$

P_2 is an ordinary time τ mapping:

$$\begin{aligned} P_2 : \boldsymbol{R}^n &\to \boldsymbol{R}^n \\ \boldsymbol{x}_1 &\mapsto \varphi((k+1)\tau, \boldsymbol{x}(k\tau), \lambda). \end{aligned} \tag{7}$$

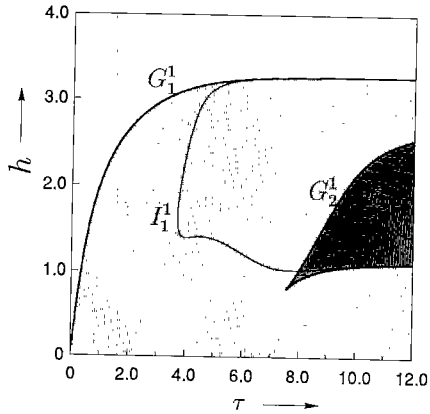

Fig. 3 Bifurcation diagram of periodic solutions in (τ-h) plane. $\kappa = 0.2$.

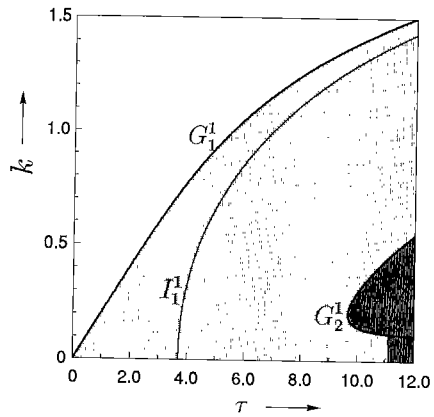

Fig. 4 Bifurcation diagram of periodic solutions in (τ-k) plane. $h = 2.0$.

Hence the Poincaré mapping P is described by:

$$\begin{aligned} P : \boldsymbol{R}^n &\to \boldsymbol{R}^n \\ \boldsymbol{x} &\mapsto P(\tau, \boldsymbol{x}, \lambda) = P_2 \circ P_1(\tau, \boldsymbol{x}, \lambda). \end{aligned} \tag{8}$$

We use this composite mapping and its derivatives to calculate not only fixed or periodic points and bifurcation parameters, but also the gain of controller stabilizing chaotic state.

4. Bifurcation Diagrams

For simplicity, we fix the parameter B_0 as 0. In this case, there exist a sink$(0, 0)$ and a saddle$(\pi, 0)$ in $S^1 \times \boldsymbol{R}$ with $h = 0$. Figures 3 and 4 show bifurcation diagrams in the τ-h and τ-k plane. In the following we fix $h = 2.0$, $\kappa = 0.2$. G_i^1 and I_i^1 $i = 1, 2$ indicate tangent and period doubling bifurcations for the fixed point, respectively. Almost regions of these diagrams there exist revolving solutions, see Fig. 5. The oscillatory solutions are observed in the shaded regions. There also exist two kinds of oscillatory solutions in the dark-shaded region, see Figs. 6 and 7. In each of the regions encircled by I_1^1 or I_2^1, there are many higher periodic and chaotic orbits.

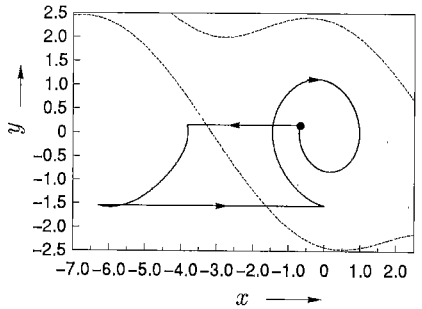

Fig. 5 Periodic orbit with a fixed point (black circle) winding around a cylindrical phase space. $\kappa = 0.2$, $h = 2.0$, $\tau = 11.8$. A straight right-oriented arrow shows taking modulo 2π and broken line shows separatrix.

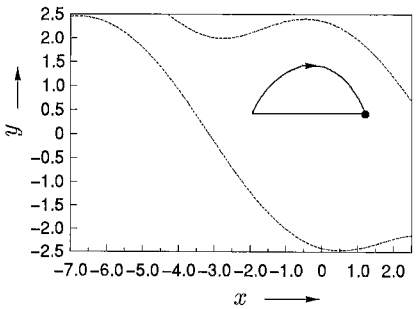

Fig. 6 Periodic orbit with a fixed point. $\tau = 3.0$.

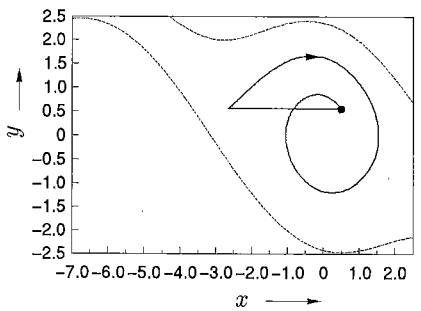

Fig. 7 Periodic orbit with a fixed point. $\tau = 10.0$.

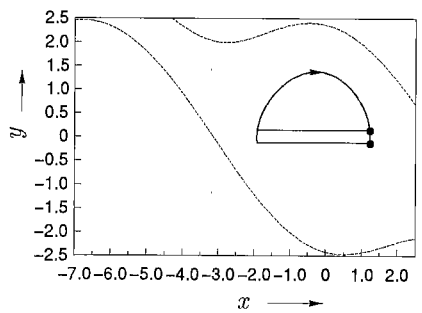

Fig. 8 2-periodic orbit bifurcated by I_1^1. $\tau = 3.32$.

Figures 8–10 show the orbits bifurcated by the cascade of period doubling. Figure 11 is a chaotic orbit winding around S^1.

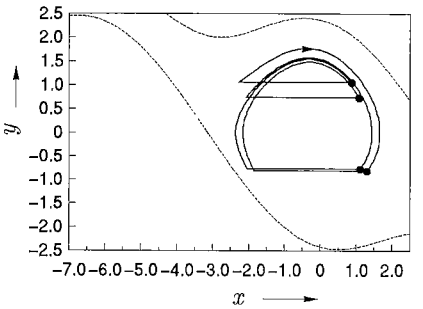

Fig. 9 4-periodic orbit. $\tau = 4.16$.

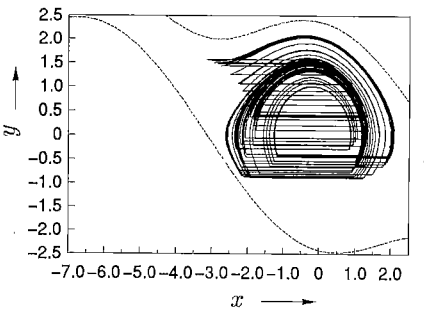

Fig. 10 Chaotic orbit bifurcated by the cascade of period doubling. $\tau = 4.24$.

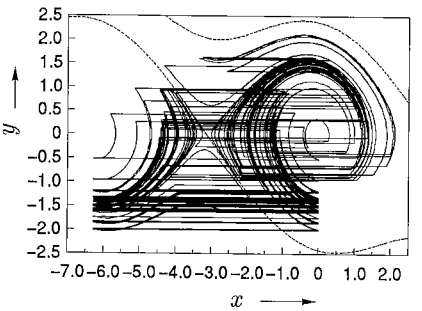

Fig. 11 A chaotic orbit winding around a cylindrical phase space. $\kappa = 0.2$, $h = 2.0$, $\tau = 4.32$.

5. Controlling the Unstable Orbit

In this section, we consider a control strategy of any periodic orbit included in Eq. (2) by applying a technique of controlling chaos [4], [5].

Suppose that the system (2) has a fixed point, i.e., there exist $\boldsymbol{x}^* \in \boldsymbol{R}^n$ and $\lambda^* \in \boldsymbol{R}$ such that

$$\boldsymbol{x}^* = P(\tau, \boldsymbol{x}^*, \lambda^*). \tag{9}$$

We call this point the target.

The variational equation in the neighborhood of the target $\boldsymbol{x}^*$ is described as follows:

$$\boldsymbol{x}(k\tau) = \boldsymbol{x}^* + \boldsymbol{\xi}(k), \quad \lambda = \lambda^* + u(k) \tag{10}$$

where, k is an integer, $u(k)$ is the perturbation of λ^*. From Eq. (9), we have

$$\boldsymbol{x}^* + \boldsymbol{\xi}(k+1) = P\left(\tau, \boldsymbol{x}^* + \boldsymbol{\xi}(k), \lambda^* + u(k)\right)$$

$$= P(\tau, \boldsymbol{x}^*, \lambda^*) + \boldsymbol{A}\boldsymbol{\xi}(k) + \boldsymbol{b}u(k) + \cdots \quad (11)$$

where,

$$\boldsymbol{A} = \left.\frac{\partial P}{\partial \boldsymbol{x}}\right|_{\boldsymbol{x}=\boldsymbol{x}^*,\ \lambda=\lambda^*} \qquad \boldsymbol{b} = \left.\frac{\partial P}{\partial \lambda}\right|_{\boldsymbol{x}=\boldsymbol{x}^*,\ \lambda=\lambda^*}. \quad (12)$$

Thus, we obtain a linearized difference equation in the neighborhood of the target as follows:

$$\boldsymbol{\xi}(k+1) = \boldsymbol{A}\boldsymbol{\xi}(k) + \boldsymbol{b}u(k). \quad (13)$$

Note that the matrices $\boldsymbol{A}$ and vector $\boldsymbol{b}$ are obtained numerically by solving the following differential equations from $t = 0$ to $t = \tau$:

$$\frac{d}{dt}\frac{\partial P}{\partial \boldsymbol{x}} = \frac{\partial \boldsymbol{f}}{\partial \boldsymbol{x}}\frac{\partial P}{\partial \boldsymbol{x}} \quad \text{with} \quad \left.\frac{\partial P}{\partial \boldsymbol{x}}\right|_{t=0} = I$$
$$\frac{d}{dt}\frac{\partial P}{\partial \lambda} = \frac{\partial \boldsymbol{f}}{\partial \boldsymbol{x}}\frac{\partial P}{\partial \lambda} + \frac{\partial \boldsymbol{f}}{\partial \lambda} \quad \text{with} \quad \left.\frac{\partial P}{\partial \lambda}\right|_{t=0} = 0. \quad (14)$$

These equations are already calculated to obtain the fixed point or bifurcation set by using the Poincaré mapping (8). We construct the state feedback to control Eq. (13):

$$u(k) = \boldsymbol{c}^\top \boldsymbol{\xi}(k) \quad (15)$$

where, $\boldsymbol{c}$ is a control vector $(1 \times n)$, and $\top$ indicates a transposition. As is well known, if

$$\det[\boldsymbol{b}|\boldsymbol{A}\boldsymbol{b}|\cdots|\boldsymbol{A}^{n-1}\boldsymbol{b}] \neq 0, \quad (16)$$

then Eq. (13) is controllable by Eq. (15). Consequently, we can choose a control vector determined by the solution of the pole assignment problem for characteristic equation:

$$\det[\boldsymbol{A} + \boldsymbol{b}\boldsymbol{c}^\top - \mu I] = 0 \quad (17)$$

where, I is an identity matrix. Finally, the composite dynamical system [5] for Eq. (2) is described as follows:

$$\frac{d\boldsymbol{x}}{dt} = \boldsymbol{f}\left(t, \boldsymbol{x}(t), \lambda^* + \boldsymbol{c}^\top(\boldsymbol{x}(k\tau) - \boldsymbol{x}^*)\right)$$
$$\text{with} \quad k\tau \leqq t < (k+1)\tau$$
$$\boldsymbol{x}(k\tau) - \boldsymbol{x}^* = [\boldsymbol{A} + \boldsymbol{b}\boldsymbol{c}^\top](\boldsymbol{x}((k-1)\tau) - \boldsymbol{x}^*). \quad (18)$$

Note that the control input calculated by (15) is applied constantly to the system parameter λ during the period τ, see Fig. 12.

In general, some methods for controlling chaos uses a property that the neighborhood of target will be visited before long by the chaotic orbit while wandering in the attractor. Equation (18) is also designed that the control is done if the orbit satisfies the following condition:

$$||\boldsymbol{x}(k\tau) - \boldsymbol{x}^*|| < \epsilon, \quad \epsilon > 0. \quad (19)$$

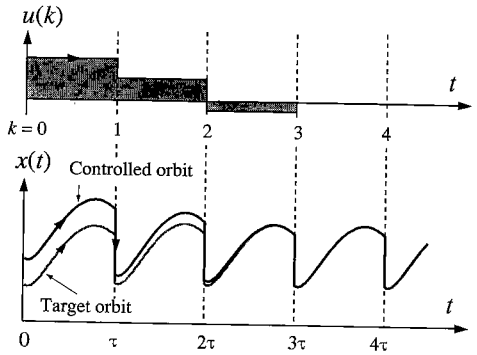

Fig. 12 Response of the state and the control input.

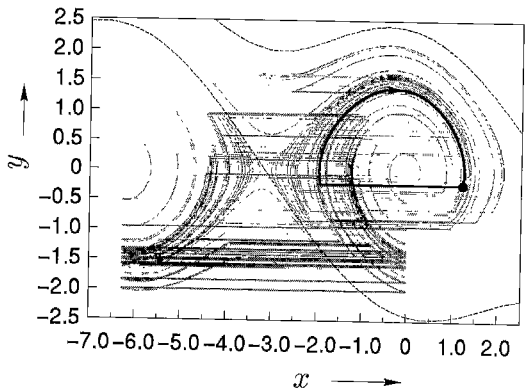

Fig. 13 Stabilized periodic orbit (thick curve). $\tau = 4.32$, $\epsilon = 0.01$. The original eigenvalues for the fixed point are $\mu_1 = -0.2868$, $\mu_2 = -1.4697$.

In case that the system parameter having a stable orbit varies to the destabilizing (bifurcation) direction, we can suppress it if the controller is designed instantly. Therefore a robust operation is achieved in wide parameter region compared with the non-controlled system. Note that the control available region called basin of attraction depends on $\boldsymbol{f}$, ϵ and assigned poles [6].

Figure 13 shows a stabilized unstable periodic orbit with fixed point embedded in a chaotic attractor by small perturbations of h. Its poles are assigned to 0 (dead beat control). We also confirm that any oscillatory and revolving solution with a fixed point can be controlled by h or B_0 if Eq. (16) is held.

6. Failure of the Stepping Motor and Its Control

Stepping motors have been used in many position and speed control systems. However, there are failure operations called pull-out depending on parameters of the motor. An analysis for the failure model of the stepping motor is studied in Ref. [7]. In this section, we derive the equation of motions for the stepping motor, and show that the equation on the velocity error plane is identical to Eq. (2). Moreover, we investigate the characteristics of the motor driven by the intermit-

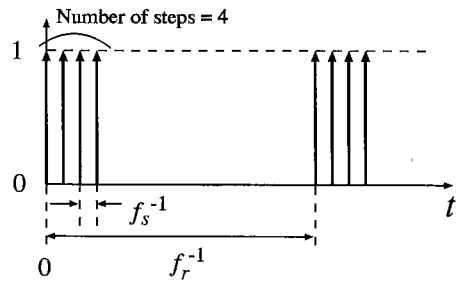

Fig. 14 Intermittent drive sequence. f_s is the stepping rate, f_r is the repetitive frequency.

tent sequence shown in Fig. 14.

6.1 The Equation of Motion and Velocity Error Plane

The torque equation of two-phase hybrid stepping motor is described by the following differential equation:

$$J\frac{d^2\theta}{dt^2} + D\frac{d\theta}{dt} + T_L = \sqrt{2}KI_m \sin\{N(U(t) - \theta)\} \tag{20}$$

where,

J [kg·cm·s^2]	the moment of inertia
D [kg·cm/rad/s]	viscous friction coefficient
T_L [kg·cm]	load torque
K [kg·cm/A]	torque constant
I_m [A]	maximum motor current
N	number of rotor teeth
U [rad]	mechanical angle

In Eq. (20) the stepwise function $U(t)$ corresponds to a stepping input signal:

$$U(t) = \frac{\pi h}{2N}\sum_{k=0}^{\infty} u(t - kT) \tag{21}$$

where, $u(t)$ is the unit step function. Putting $\Theta = N\theta$ we try to rewrite Eq. (21) into a normalized form as:

$$\frac{d^2\Theta}{dt^2} + \frac{D}{J}\frac{d\Theta}{dt} + \frac{N\sqrt{2}KI_m}{J}\sin\{\Theta - NU(t)\} + \frac{N}{J}T_L = 0. \tag{22}$$

By scaling the time axis as $t' = \omega t$, Eq. (22) becomes

$$\frac{d^2\Theta}{dt'^2} + \kappa\frac{d\Theta}{dt'} + \sin\left\{\Theta - NU\left(\frac{t'}{\omega}\right)\right\} + B_0 = 0 \tag{23}$$

where

$$\omega = \sqrt{\frac{N\sqrt{2}KI_m}{J}}$$
$$\kappa = \frac{D}{\sqrt{N\sqrt{2}KI_m J}}$$
$$B_0 = \frac{T_L}{\sqrt{2}KI_m}. \tag{24}$$

Finally, by changing the variables in Eq. (23) such that

$$t = t',\ x = \Theta - NU\left(\frac{t'}{\omega}\right),\ y = \frac{d\Theta}{dt} \tag{25}$$

Eq. (22) is normalized as

$$\frac{dx}{dt} = y - \frac{\pi}{2}\sum_{k=0}^{\infty}\delta(t - k\omega T)$$
$$\frac{dy}{dt} = -\kappa y - \sin x - B_0$$
$$x(0) = y(0) = 0. \tag{26}$$

This equation is equivalent to Eq. (2) with $h = \omega = 1$ and its phase space (x, y) is called the velocity error plane [7].

After the transient state, if the orbit of Eq. (26) stays at $0 \leqq x < 2\pi$ as $t \to \infty$ without taking modulo 2π, the normal operation is almost achieved. If the orbit is jumped across left separatrix one by one then the system behaves the asynchronous oscillation called pull-out operation. Figure 5 is also classified into this operation. One of our objectives of this study is to clarify this phenomenon depending on system parameters by using bifurcation theory.

6.2 Characteristics of Intermittent Drive

In industrial fields, there exist many demands of the mechanism which accomplishes the synchronized operation for other intermittent motions, e.g., paper feeder, sawing machine, etc. The stepping motor driven by the intermittent sequence as shown in Fig. 14 is suitable to realize such motions. Reference [2] suggests that some choices of the stepping rate f_s and repetitive frequency f_r involve pull-out. In this section, we investigate these phenomena by bifurcation theory, and control them by using the method discussed in Sect. 5.

We fix the parameters as follows:

$$J = 1.12\times10^{-3},\ D = 0.2,\ T_L = 0,\ \sqrt{2}KI_m = 22$$

and the number of steps during a period is 4. Thus the natural frequency and damping are as follows:

$$f_n = \omega/2\pi \approx 158\,[\text{Hz}]$$
$$\kappa \approx 0.18.$$

Figure 15 shows the bifurcation diagram of periodic solutions driven by intermittent sequences in f_s-f_r plane. In this figure, the line A indicates

$$f_r = \text{number of steps} \times f_s. \tag{27}$$

The drive sequence on A is identical to Fig. 2, i.e., the impulses are arranged in equally interval. Therefore, the intermittent driving is achieved under this line. In light-shaded region under A there exist stable oscillatory or revolving orbits with a fixed point. In dark-shaded region enclosed G^1 and I^1 these orbit are bifurcated to

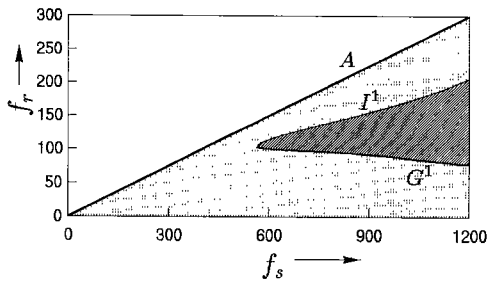

Fig. 15 Bifurcation diagram of periodic orbit driven by intermittent drive sequence.

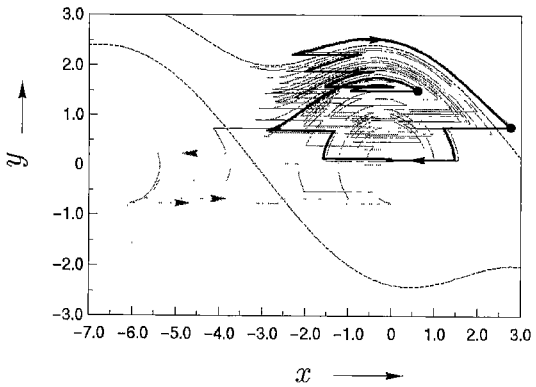

Fig. 16 2-period stable orbit started from the origin. The shaded line shows transient state. $\kappa = 0.18$, $f_r = 198.2$ Hz, $f_s = 1982$ Hz.

chaotic revolving orbits. Figure 16 shows a 2-period orbit bifurcated by I^1. The neighborhood of the point crossing G^1 and I^1 we cannot trace the both bifurcation curves anymore because many higher periodic revolving and oscillatory solutions are found around there by changing severe parameter perturbations.

Note that Fig. 15 is not considered the starting characteristics. The orbit started from $(x_0, y_0) = (0, 0)$ does not always converge to the stable oscillatory orbit; in other words, it may not realize the normal operation.

6.3 Controlling Pull-Out

In Sect. 5 a control method suppressing bifurcations for original stable target is proposed. We can also apply this method to the intermittent drive stepping motor. In this section, we propose a controller satisfying the following specifications:

- Avoid the pull-out.
- Consider the starting characteristics.

The latter condition indicates that the orbit started from initial state $(x_0, y_0) = (0, 0)$ should fall into the target orbit to achieve the normal operation. At the steady state, if the orbit started from the origin falls into a stable revolving orbit, then it can be regarded as pull-out.

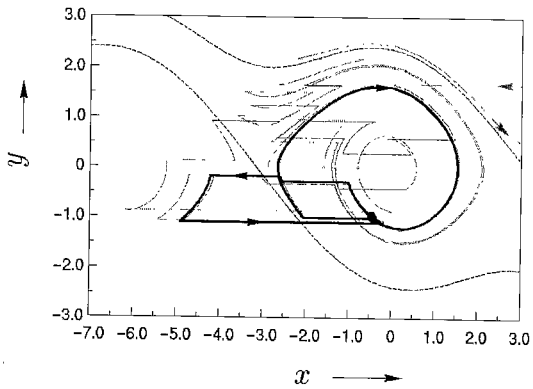

Fig. 17 Pull-out orbit(thick curve) and the fixed point. $\kappa = 0.18$, $f_r = 90$ Hz, $f_s = 900$ Hz.

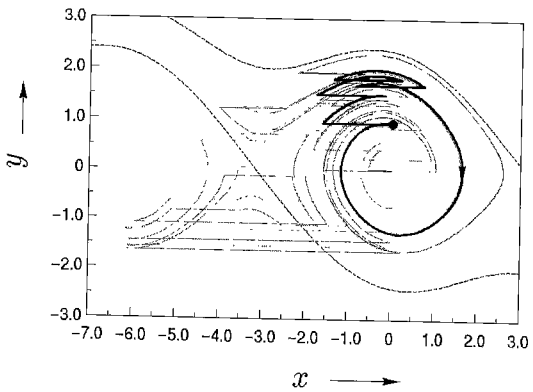

Fig. 18 Stabilized orbit. Both poles are assigned to 0. $\epsilon = 2.0$.

Figure 17 shows pull-out started from the origin. In the same system parameters there also exists a basin falling into the stable oscillatory target. To avoid this starting failure we manipulate the basin of attraction for stable target by developing a compensator.

The compensator designed by same method discussed in Sect. 5 gives an opportunity to change the attractor into which the orbit falls and improves the transient response by manipulating poles of the characteristic equation for the stable target. We choose $1/f_r$ which allows large scale perturbations, as the control parameter to enlarge the control area ϵ because the control value is proportional to the deviation ξ. Thus the compensator changing timings of adding input sequences. Note that we assume the ratio f_s/f_r is constant. Figure 18 shows the case that both poles of the compensator assigned to 0, but several times the orbit winding around S^1. On the other hand, Fig. 19 shows a satisfactory example which poles are assigned to 0 and -0.5. The control value is perturbed within 16.5% for $1/f_r$. For practical use, we should investigate a compensator using the fixed stepping rate.

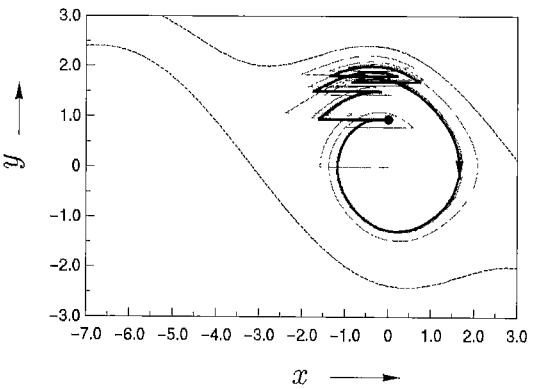

Fig. 19 Improved transient state. The poles are assigned to 0 and -0.5. $\epsilon = 1.0$.

7. Conclusions

We investigate some properties of Eq. (2) by using bifurcation diagrams. In this system, there exist the revolving and oscillatory solutions, and chaotic solutions are caused by their bifurcations. We also propose a method to control the target orbit by small perturbations of the system parameter, and show an example of controlling. Further, we study the properties of the stepping motor by using velocity error plane. In case that the motor driven by intermittent impulse sequences, there exist failure operations called pull-out operations. Then we construct a compensator to avoid them by changing the intermittent driving frequency and stepping rate, and illustrate some examples applied the pole assign technique. To develop the actual implementations is a future problem.

References

[1] O. Morimoto and H. Kawakami, "Bifurcation diagram of a BVP equation with impulsive external force," Proc. Symposium on Nonlinear Theory and its Applications (NOLTA '94), pp.205–208, Oct. 1994.

[2] I. Morita and T. Hojo, "Intermittent drive characteristics of hybrid stepping motor," Proc. of Small Motor International Conference (SMIC '93), pp.113–118, July 1993.

[3] S. Doi and S. Sato, "The global bifurcation structure of BVP neural model driven by periodic pulse trains," IEICE Technical Report, CAS92-91, 1993.

[4] F. Romeiras, C. Grebogi, E. Ott, and W. Dayawansa, "Controlling chaotic dynamical systems," Physica, vol.D, no.58, pp.165–192, 1992.

[5] T. Ueta and H. Kawakami, "Composite dynamical system for controlling chaos," Trans. IEICE, vol.E78-A, no.6, pp.708–714, 1995.

[6] H. Kawakami and T. Ueta, "Controlling theory as applied to controlling chaotic dynamical systems," IECE Technical Report, NLP94-63, 1994.

[7] C. Taft and R. Guthier, "Stepping motor failure model," IEEE Trans. Ind. Electron. Contr. Instrum., vol.AC-13, no.3, pp.464–474, 1969.

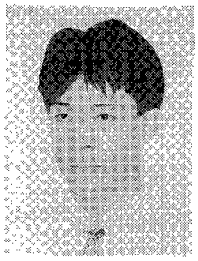

Tetsushi Ueta was born in Kochi, Japan, on March 1, 1967. He received the B.Eng. in electronic engineering, and M.Eng. in electrical engineering from the University of Tokushima, Tokushima, Japan, in 1990, and 1992, respectively. Since 1992, he was been Research Associate of Information Science and Intelligent Systems, the University of Tokushima. His interest is bifurcation problems of dynamics.

Hiroshi Kawakami was born in Tokushima, Japan, on December 6, 1941. He received the B.Eng. degree from the University of Tokushima, Tokushima, Japan, in 1964, the M.Eng. and Dr.Eng. degrees from Kyoto University, Kyoto, Japan, in 1966 and 1974, respectively, all in electrical engineering. Presently, he is Professor of Electrical and Electronic Engineering, the University of Tokushima, Tokushima, Japan. His interest is qualitative properties of nonlinear circuits.

Ikuro Morita received the B.E. and M.E. degrees in electrical engineering from the University of Tokushima, in 1969 and 1971,respectively, and the Ph.D. degree in electrical engineering from Kyoto University in 1990. Since 1972 he has been with the Department of Electrical Engineering, the University of Tokushima, where he is currently an Associate Professor. His current research interests include fault diagnosis, analysis, and control of electrical machines. Dr. Morita is a member of the IEEE.